scientific reports

Check for updates

OPEN

A quantitative assessment of the hand kinematic features estimated by the oculus Quest 2

Daniele Borzelli[1,4], Vittorio Boarini[2] & Antonino Casile[1,3]✉

In the past decade, immersive virtual reality (VR) has garnered significant interest due to its capacity to ability a strong sense of presence and allow users to act in virtual environments. In particular, VR has been increasingly used in clinical settings to present scenarios for motor rehabilitation purposes. Existing research efforts mostly focus on investigating the clinical effectiveness of different routines. However, modern VR systems, in addition to presenting scenarios, also have hand motion tracking capabilities that could be potentially used to gather clinically relevant kinematic data from the patients while they execute the VR tasks. Here, we quantitatively assess the capability of tracking hand movements of a popular VR system, the Oculus Quest 2 by Meta, by comparing its kinematic measures with those provided by a commercial marker-based motion capture system. Our findings suggest that the Quest 2 provides reasonably reliable estimates of hand position and velocity. Estimates of acceleration are noisier and might be sometime unsuitable for kinematic assessments. Notably, the accuracy of the kinematic estimates varies across spatial directions. Estimates along the left/right direction are the most accurate, followed by estimates along the up/down axis. Estimates along the near/far axis appear to be the noisiest. Furthermore, we also found that Quest 2 can provide fine-grained measures of grip aperture, but the precision of these measures might be affected by the subject's head movements while wearing the system. Our results suggest that modern VR devices, in addition to presenting immersive scenarios, could be potentially used in rehabilitation settings also to provide clinically relevant kinematic measures that can potentially inform medical decisions.

In the last decade, the field of immersive virtual reality (henceforth VR) has experienced dramatic growth going from laboratory prototypes to robust, off-the-shelf products. Devices based on head-mounted displays (henceforth HMD), such as the Oculus Quest from Meta (Menlo Park, USA) or Vive (HTC, Xindian, New Taipei, Taiwan) have entered our houses for recreational or educational purposes. An HMD is a device that is worn on the head, binocularly displays a virtual environment and, in some models, lets the user interact with virtual objects. In particular, modern HMDs are designed so as to allow users to experience virtual environments with a strong sense of presence (i.e., the feeling of "being there" in the virtual scenario), plausibility (i.e., the feeling that events in the virtual environment are "really happening"), and embodiment (i.e., the feeling that the body the user has in the virtual environment is "really" hers/his)[1] (for a recent review see[2]).

In addition to presenting a virtual environment, modern HMDs can also track, in real time, the movements of the subjects' hands to allow the users to interact with virtual objects. For example, in the HTC VIVE this is achieved by tracking the position of special markers anchored to the body while the Oculus Quest estimates the position and posture of the user's hands by using cameras placed on the front of the HMD and proprietary computer vision algorithms. This additional feature, encouraged researchers to employ HMD in their experimental protocols also as tracking tools and therefore to use them in the research practice[3–5].

Notably, kinematic assessments are widely used in clinical settings to characterize the amount of impairment and subsequently to monitor motor recovery[6–9].

The increasing rate of adoption of VR devices has prompted the research community to explore new ways in which they could be employed. For example, the flexibility in presenting sensory stimulation and motor tasks offered by virtual environments has paved the way for the use of VR devices in cognitive[10–17] and motor[18–21] research. Furthermore, many research efforts are presently focused on the use of HMDs in clinical settings[22–25] and, in particular, for the motor rehabilitation of neurological disorders such as multiple sclerosis[26] or stroke[27].

[1]Department of Biomedical and Dental Sciences and Morphofunctional Imaging, University of Messina, 98124 Messina, Italy. [2]Department of Mathematics and Computer Science, University of Ferrara, 44121 Ferrara, Italy. [3]Istituto Italiano di Tecnologia, Center for Translational Neurophysiology of Speech and Communication, 44121 Ferrara, Italy. [4]IRCCS Fondazione Santa Lucia, 00179 Rome, Italy. ✉email: antonino.casile@unime.it; toninocasile@gmail.com

Motor rehabilitation is a complex process requiring the identification of specific tasks tailored to the patient's abilities[28]. These tasks are carefully calibrated for motor variability and complexity based on individual capabilities. Once the patient-specific rehabilitation plan is defined, motor therapy focuses on the repetitive execution of simple tasks, enabling gradual skill acquisition and improvement. While such training has been found to maximally stimulate neuroplasticity[29], and thus induce motor recovery[30], given its repetitive nature, it can quickly become boring and cumbersome for the patients and it might result in severe adherence issues[31]. Additionally, the therapist's constant presence, necessary to monitor rehabilitation progress and adjust it based on actual outcomes, limits the time when a patient can practice physiotherapy to the therapist's availability and increases the overall cost[32]. To address these issues, immersive VR-based systems have been proposed in the literature that offer engaging, yet enjoyable and varied, scenarios and tasks designed with rehabilitation purposes[33–36], for a recent review see[37], These systems might contribute to increase patients' engagement, they might perform some automatic assessments, thus partially unloading the therapist, and they could be used at home, thus increasing the dosage of the rehabilitation therapy.

In particular, the motion-tracking capabilities of the Quest 2 open up the possibility to use HMDs not only for delivering serious games in an immersive and engaging way but also for clinical applications[38–40]. This system belongs to a new generation of devices that are known to substantially reduce, or even completely eliminate motion sickness or other sources of discomfort in virtual environments[41] and it has high-end technical specifications that support real-time perception and enhanced immersion in virtual scenarios. In addition, compared to the HTC VIVE, The Quest 2 needs no additional hardware for motion tracking (the VIVE uses so-called "Trackers") and is significantly less expensive, which might be important for potential widespread adoption in clinical settings. Furthermore, the Oculus Quest 2 has demonstrated greater accuracy than both the Oculus Quest[42] and SteamVR Tracking 2.0 [43]. It has been shown that the Oculus Quest 2 can accurately estimate head position and orientation in static conditions or over short distances[43], is suitable for analyzing navigation during locomotion[44], and reliably tracks the position of its handheld controllers[45,46]. It has also been suggested as a valuable tool for monitoring shoulder kinematics during rehabilitation[39].

In a previous study, we exploited the motion tracking features of the Oculus Quest 2 to develop an immersive VR system in which stroke patients could carry out rehabilitation routines directly with their virtually-rendered hands[33]. In a further study, we assessed whether Quest 2's markerless motion tracking capabilities could provide a reliable estimate of the peak velocity of the patients' hands[47], a widely used kinematic measure in clinical assessments[6,7]. We found that the estimates of peak hand velocity produced by the Oculus Quest 2 strongly correlated with their ground-truth values estimated by means of an expensive state-of-the-art marker-based motion capture system[47].

The goal of the present study is to provide a comprehensive evaluation of the markerless motion capture capabilities of the Oculus Quest 2. To this end, we expanded on our previous study, and we computed a large set of kinematic measures using motion capture data provided by the Oculus Quest 2 during the performance of different types of upper-limb and hand movements. We then assessed the accuracy and reliability of these measurements by comparing them with their ground-truth values computed using motion capture data simultaneously recorded (Fig. 1) by means of a marker-based commercial system (Optitrack by Natural Point Inc., Corballis, OR, USA).

Results

The Oculus HMD tracks hand movements by filming the hands with its cameras, segmenting these images from the background and fitting these segmented images with a kinematic model (Table S1). These cameras are positioned at the four corners of the HMD and they thus move with the head. In a preliminary experiment,

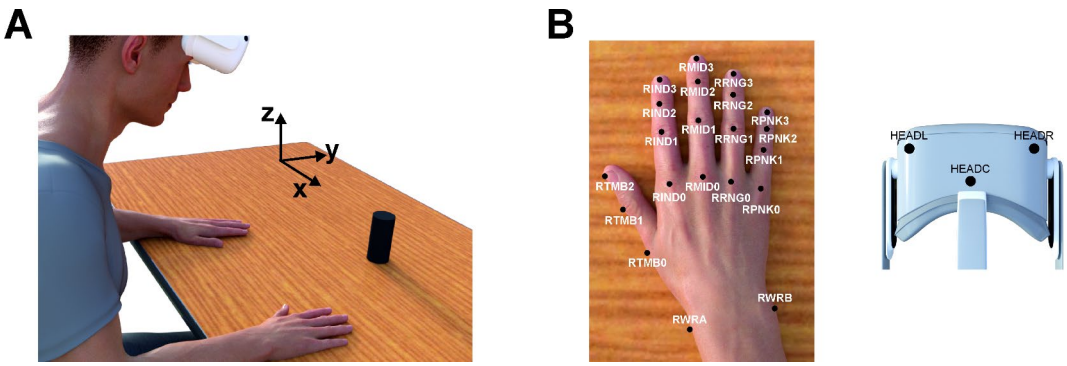

Fig. 1. Experimental setup – (**A**) Graphical depiction of the experimental setup. The participant sat in front of a table and performed different hand actions. In one condition, he wore a head-mounted display at the top of his head to have a normal view of the table in front of him. In another condition (not shown in the figure) the HMD was tethered on a tripod positioned close to the participant's body. During action performance the kinematics of head and hand movements were recorded by means of the Oculus' motion tracking capabilities and a commercial marker-based optical system (Optitrack). (**B**) Placement of the infrared reflective markers used by the Optitrack system. A total of 21 markers were placed on the main hand joints and 3 markers were placed on the HMD to record head movements.

we assessed that there could be conditions producing cross talks between head and hand movements, with head movements mistakenly interpreted by the Oculus Quest 2 as hand movements (Fig. 7). For this reason, we performed all our experiments in two conditions. That is, when the Oculus (1) was tethered to a tripod placed very close to the participant's body ("tethered" condition) and (2) was worn on the participant's head ("untethered" condition).

The precision of position estimates provided by the Quest 2 is not homogeneous in space

In our first experiment we measured arm kinematics during center-out reaching movements, a widely used task in motor control studies (see, for example[48]), To this end, we measured the position of the subject's right hand while he was performing reaching movements from a central hand rest position to three different positions arranged to his left, frontally and to his right (Fig. 2A). On each trial, we computed, both from Oculus and Optitrack data, the movement length defined as the distance traveled by the hand from its starting to its final position. Figure S1 shows the hand trajectory and the average velocity profiles for all trials.

The left panel of Fig. 2B shows the distributions of traveled distances estimated from Oculus (red) and Optitrack (blue) data in the tethered condition. The mean traveled distance (Oculus: leftward = 18.2 ± 0.63; frontal = 19.5 ± 0.9; rightward = 18.8 ± 0.68 – Optitrack: leftward = 18.1 ± 0.47; frontal = 20.4 ± 0.57; rightward = 18.6 ± 0.38) estimated from Oculus data was significantly smaller than that estimated from Optitrack data for frontal movements but not significantly different for leftward and rightward movements (leftward: T = 85, p-value = 0.47; frontal: T = 3, p-value = 9.5 10^{-6}; rightward: T = 60, p-value = 0.1 - Wilcoxon signed rank test). The mean ratio of the Oculus and Optitrack estimates were 1.0 ± 0.01, 0.96 ± 0.02, and 1.01 ± 0.02 for leftward, frontal, and rightward movements respectively. The scaling factors, that represent the dispersion around the median, of the Oculus and Optitrack distributions of traveled distance were not significantly different across all conditions (leftward: statistics = 179, p-value = 0.1; frontal: statistics = 187, p-value = 0.22; rightward: statistics = 178, p-value = 0.08; Ansari-Bradley test). The right panel of Fig. 2B shows the scatterplot of hand traveled distances estimated from Oculus and Optitrack data. For all three movement directions, the Oculus and Optitrack measurements were significantly correlated (leftward: ρ = 0.98, p-value = 3.7 10 − 14; frontal: ρ = 0.84, p-value = 3.8 10 − 6; rightward: ρ = 0.88, p-value = 2.3 10 − 7 - Spearman's rank correlation) and they were well fit by a linear model (leftward: slope = 0.72, R^2 = 0.97; frontal: slope = 0.57, R^2 = 0.9; rightward: slope = 0.49, R^2 = 0.88).

The left panel of Fig. 2C shows the distributions of traveled distances derived from Oculus (red) and Optitrack (blue) data in the untethered condition (Oculus: leftward = 17.9 ± 0.48; frontal = 19.7 ± 0.72; rightward = 19.2 ± 0.76 – Optitrack: leftward = 18.3 ± 0.56; frontal = 21.3 ± 0.67; rightward = 18.9 ± 0.43). In this case, the mean distances computed from Oculus and Optitrack data were significantly different for all movement directions (leftward: T = 0, p-value = 1.9·10^{-6}; frontal: T = 0, p-value = 1.9·10^{-6}; rightward: T = 50, p-value = 0.04 - Wilcoxon signed rank test). The mean ratio of the Oculus and Optitrack estimates were 0.98 ± 0.007, 0.93 ± 0.01, and 1.01 ± 0.02 for leftward, frontal, and rightward movements respectively. The scaling ratio of their distributions were not significantly different across all three directions of hand motion (leftward: statistics = 216, p-value = 0.77; frontal: statistics = 210, p-value = 1.0; rightward: statistics = 179, p-value = 0.1; Ansari-Bradley test). Also in this case, for all three movement directions, the Oculus and Optitrack measurements were significantly correlated (leftward: ρ = 0.97, p-value = 2.65·10^{-12}; frontal: ρ = 0.93, p-value = 1.8·10^{-9}; rightward: ρ = 0.78, p-value = 4.4·10^{-5} - Spearman's rank correlation) and they were well fit by a linear model (leftward: slope = 1.13, R^2 = 0.97; frontal: slope = 0.88, R^2 = 0.92; slope = 0.49, rightward: R^2 = 0.87).

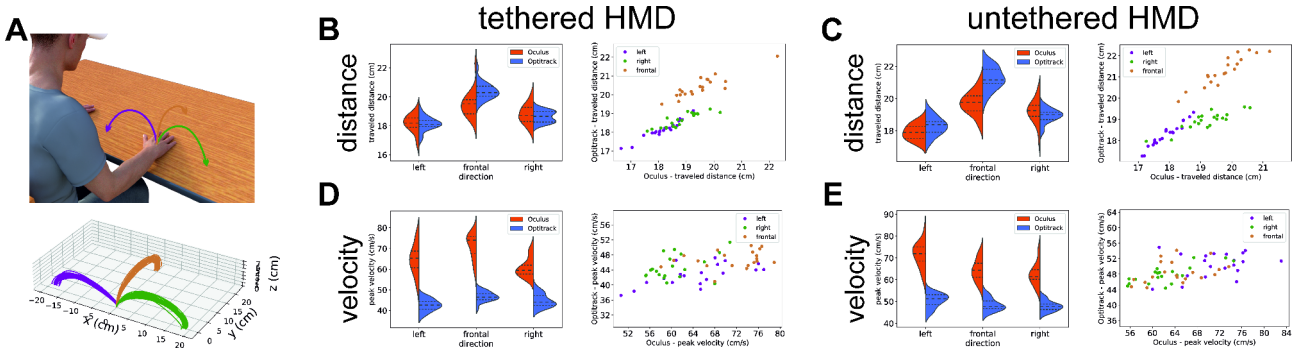

Fig. 2. Traveled distance and peak velocity during center-out reaching movements – (**A**) Experimental paradigm. The subject executed reaching movements from a central position to three different end positions to his left (purple curves) and right (green curves) and in front of him (dark yellow curves). (**B**) Violin plots (left) and scatterplots (right) of the hand traveled distances during the reaching movements as estimated from Oculus (red) and Optitrack (blue) data in the tethered condition for each of the three endpoint positions. (**C**) Hand traveled distances measured in the untethered condition. Conventions and symbols are as in panel B. (**D**) Violin plots (left) and scatterplots (right) of the peak velocities during the reaching movements as estimated from Oculus (red) and Optitrack (blue) data in the tethered condition for each of the three endpoint positions. (**E**) Peak velocities measured in the untethered condition. Conventions and symbols are as in panel D. Raw position and velocity data are plotted in Figure S1.

Taken together, the results in Fig. 2B, C show that, in general, the Oculus produces estimates of the hand position (and thus its traveled distance) that, in some cases, might significantly differ from their veridical values both in their mean and standard deviations. However, the average difference is relatively small (in the range of 1–2 cm, see average values above) and, most importantly, in all investigated conditions the trial-by-trial estimates of hand traveled distance were significantly correlated with their ground-truth values. Furthermore, both in the tethered and in the untethered conditions the dispersions of the Oculus estimates were not significantly different from their ground-truth values.

The Quest 2 overestimates peak velocity during reaching movements

We next examined the peak velocity during reaching movements estimated from Oculus and Optitrack data. The peak velocity is, for example, an important indicator in clinical assessments[6,47,49]. The right columns in Figures S1 B, C show the velocity profiles for all trials and experimental conditions. In general, the velocity profiles estimated from Oculus position information were noisier than their ground-truth value and their shape (top panels in the right columns of Figure S1 B, C) differed from its ground-truth bell-shaped profile (bottom panels in the right columns of Figure S1 B, C).

As shown in Fig. 2D, E, the estimates of peak velocity derived from Oculus data (red distributions. Tethered: leftward = 65 ± 7.2; frontal = 71 ± 6; rightward = 61 ± 4.5. Untethered: leftward = 71 ± 5.7; frontal = 64 ± 5; rightward = 63 ± 5.1) were significantly higher than their veridical values (blue distributions. Tethered: leftward = 43 ± 2.8; frontal = 47 ± 2.3; rightward = 45 ± 3.2. Untethered: leftward = 50 ± 3.2; frontal = 49 ± 2.8; rightward = 48 ± 2.2) both in the tethered and untethered condition (Tethered: leftward: T = 0, p-value = $1.9 \cdot 10^{-6}$; frontal: T = 0, p-value = $1.9 \cdot 10^{-6}$; rightward: T = 0, p-value = $1.9 \cdot 10^{-6}$. Untethered: leftward: T = 0, p-value = $1.9 \cdot 10^{-6}$; frontal: T = 0, p-value = $1.9 \cdot 10^{-6}$; rightward: T = 0, p-value = $1.9 \cdot 10^{-6}$ - Wilcoxon signed rank test). with the ratio between Oculus and Optitrack estimates being 1.51 ± 0.12, 1.52 ± 0.12, and 1.36 ± 0.11 for leftward, frontal, and rightward movements respectively in the tethered condition and 1.41 ± 0.12, 1.33 ± 0.1, and 1.3 ± 0.07 for leftward, frontal, and rightward movements respectively in the untethered condition. Furthermore, the scaling ratio of their distributions was significantly different only along the leftward direction in the tethered condition and in the leftward and frontal directions in the untethered condition (Tethered - leftward: statistics = 166, p-value = 0.02; frontal: statistics = 178, p-value = 0.09; rightward: statistics = 195, p-value = 0.44 – Untethered - leftward: statistics = 166, p-value = 0.02; frontal: statistics = 173, p-value = 0.04; rightward: statistics = 179, p-value = 0.1; Ansari-Bradley test).

The right panels in Fig. 2D, E show the scatterplots of the peak velocity estimated from Oculus (x axis) and Optitrack (y axis) data. Contrary to position information, the Oculus and Optitrack measurements of peak velocitiy tended not to be correlated across trials with the only exception of leftward movements in the tethered condition and rightward movements in the untethered condition (Tethered - leftward: ρ = 0.66, p-value = 0.001; frontal: ρ = 0.36, p-value = 0.11; rightward: ρ = 0.33, p-value = 0.15 – Untethered - leftward: ρ = 0.2, p-value = 0.39; frontal: ρ = 0.39, p-value = 0.09; rightward: ρ = 0.78, p-value = $4.4 \cdot 10^{-5}$ - Spearman's rank correlation). Consequently, the R^2 values of their linear fits were lower compared to those yielded by position information (Tethered – slope = 0.26, leftward: $R^2 = 0.66$; frontal: slope = 0.11, $R^2 = 0.29$; rightward: slope = 0.3, $R^2 = 0.43$ – Untethered: leftward: slope = 0.15, $R^2 = 0.27$; frontal: slope = 0.2, $R^2 = 0.36$; rightward: slope = 0.34, $R^2 = 0.76$).

To gain a better understanding of the results of Fig. 2 we examined Oculus' trial-by-trial estimates of hand position and velocity along the different axes (Fig. 3). When examined vis-à-vis their ground-truth values they

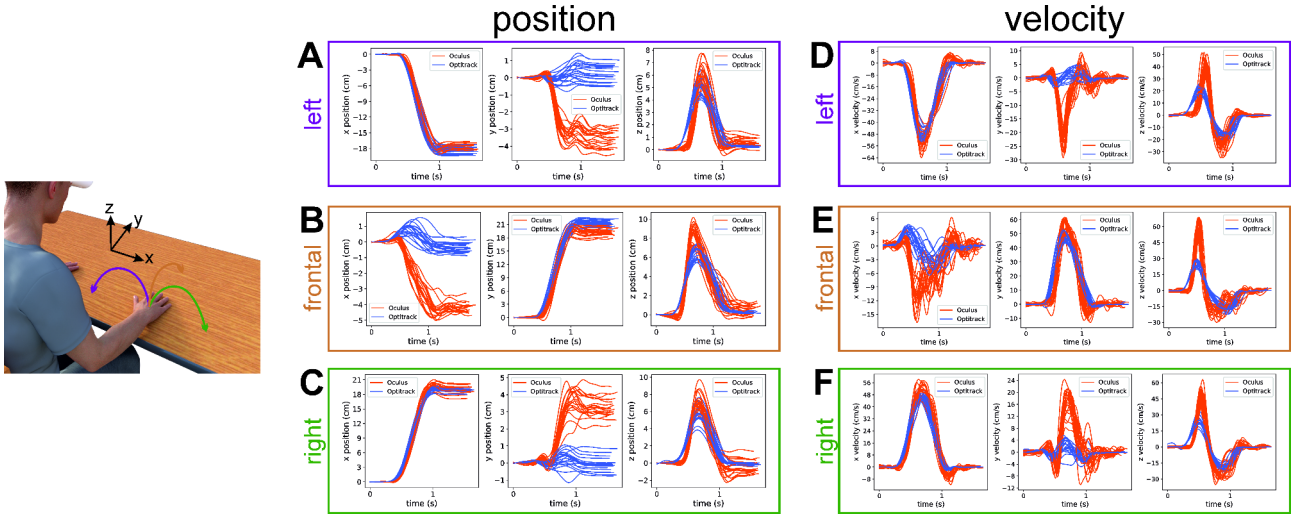

Fig. 3. Trial-by-trial position and velocity profiles during center-out reaching movements – Trial-by-trial position (**A**, **B**,**C**) and velocity (**D**, **E**,**F**) of the hand along the x, y and z axes during execution of the leftward (purple), frontal (dark yellow) and rightward (green) reaching movements in the untethered condition shown Fig. 2 (data for the tethered condition are shown in Figure S2).

revealed several characteristics of how the Oculus estimates hand kinematics. First, at the onset of the reaching movement, the Oculus exhibits an initial delay in detecting the motion of the hand. The Oculus estimates of hand position initially lag behind their veridical position (see, for example, the time points around t = 0 in the rightmost panel in Fig. 3A) and the Oculus then compensates with a "catch-up" movement (see time points around t = 0.5s in panels A, B and C). The effect of this "catching-up" process is an overshoot in the velocity profile of the hand approximately in the middle of the reaching movement (see time points around t = 0.5s in Fig. 3 panels D, E, and F). This explains the overshoot in the estimation of the peak velocity shown in Fig. 2D, E. This overshoot is potentially related to predictive computations (e.g., Kalman filtering) performed by the Oculus. These predictive computations are likely independent of the specific value of the velocity, which might explain why Oculus and Optitrack estimates of peak velocity tended to be, at least in the sample of 20 trials for each condition examined here, uncorrelated (but see[47] for results in a larger sample). Second, it appears that the Oculus exhibits also a delay in detecting that the hand has stopped. As a consequence, it overshoots the hand position when it reaches zero velocity, exhibiting then a correction towards the final veridical position (see, for example, time points around t = 1 in the left panels in Fig. 3A, B,C). This overshoot in the estimate of the hand position produces also an overshoot in the velocity compared to its veridical value toward the end of the reaching movement (see, for example, time points around t = 1 in the left panels in Fig. 3A, B,C). Third, when the movement of the hand along an axis is small (i.e. few centimeters) then the Oculus' estimates can exhibit substantial errors (see, for example, the central panel in Fig. 3A and B and the leftmost panel in Fig. 3B).

Taken together, the results of Figs. 2 and 3 suggest that the estimates of peak velocity provided by the Oculus are significantly less accurate than position information and they tend to overestimate their veridical values. This overestimation is lower in the untethered compared to the tethered condition.

Estimates of grip aperture provided by the Quest 2 are noisy but overall reliable

The Oculus does not only provide a measure of the hand trajectory, but it also fits a kinematic model to the instantaneous hand posture to recover the configuration of different joints. To assess the reliability of these joint positions we motion captured the subject while performing reach-to-grasp movement to cylinders of 3 cm and 5 cm diameters. On each trial, we estimated the grip aperture from Oculus data by computing the distance between the position of the two joints *r_index_fingernail_marker_pos*, *r_thumb_fingernail_marker_pos* (Table S1) and from Optitrack data by computing the distance between the two markers *RIND3*, *RTMB2* (Fig. 1). In the following, we analyze the distributions of the grip apertures at the end of the reaching movement when the subject was grasping the goal object. Figure S3 shows the temporal unfolding of the grip aperture during trials in which the 3 cm cylinder was grasped.

Figure 4B shows the distributions of the final grip apertures in the tethered conditions. Both Oculus and Optitrack estimates of the grip aperture correlated well with the actual diameter of the goal object (Oculus – 3 cm cylinder: 4.14 ± 0.34; 5 cm cylinder: 6.7 ± 0.27. Optitrack: 3 cm cylinder: 5.2 ± 0.17; 5 cm cylinder: 7.2 ± 0.19). It is not meaningful to compare the averages of the Oculus and Optitrack distributions since the two considered joints

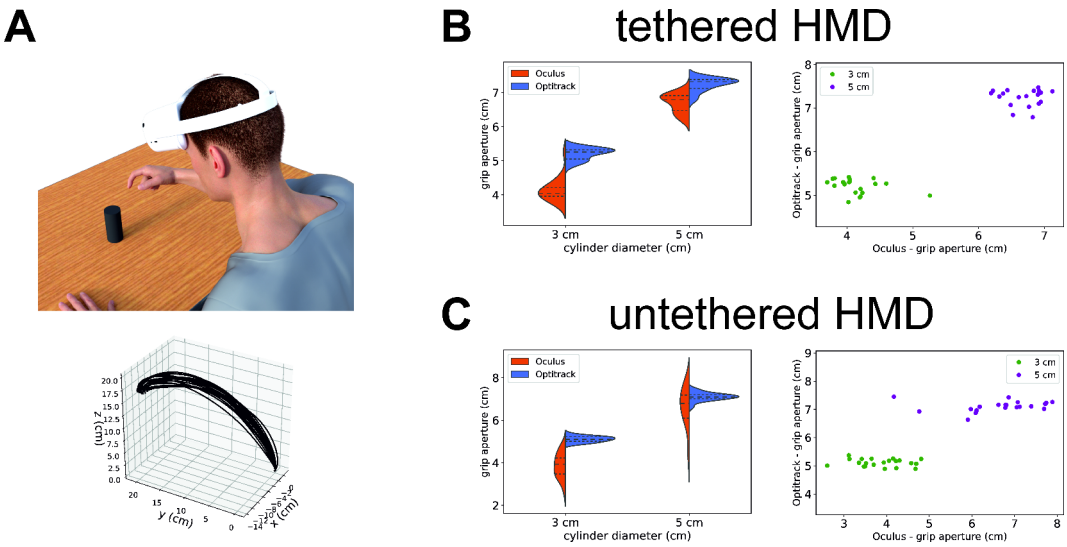

Fig. 4. Grip aperture during reach-to-grasp movements – (**A**) Experimental paradigm. The subject executed reach-to-grasp movements from a central position to two a cylinder having a diameter of either 3–5 cm. The curves in the bottom panel represent the position of the wrist during one of the experimental sessions. (**B** – left panel) Distributions of the grip aperture measured at the end of the movement when the subject's fingers were grasping the goal object. Grip aperture was computed from Oculus (red) and Optitrack (blue) data in the tethered condition. (**B** – right panel) Scatterplot of the same data shown in the left panel. Green and purple dots indicate grip apertures measured when the subject was grasping the 3 cm and 5 cm cylinder respectively. (**C**) Distributions (left) and scatterplot (right) of the grip apertures measured in the tethered condition. Conventions and symbols are as in panel B.

of the Oculus hand model and the considered Optitrack markers were not matched to the same physical position on the hand. They thus index two different distances that do not necessarily need to have the same average. It is, however, meaningful to compare the scaling ratio of the two distributions to assess the relative precision of the measurements of grip aperture. In the tethered condition, these ratios were significantly different in the 5 cm but not in the 3 cm condition (3 cm: statistic = 187, p-value = 0.23; 5 cm: statistic = 161, p-value = 0.008). In the untethered condition (Oculus – 3 cm cylinder: 3.9 ± 0.6; 5 cm cylinder: 6.6 ± 0.97. Optitrack: 3 cm cylinder: 5.1 ± 0.13; 5 cm cylinder: 7.1 ± 0.18), however, the scaling ratios were significantly different for both the 3 cm and the 5 cm object (3 cm: statistic = 148, p-value = 0.3.4 10^{-5}; 5 cm: statistic = 150, p-value = 0.0009;) . As a consequence, in the scatterplot of Oculus vs. Optitrack estimates of grip aperture the dots exhibited a larger "spread" along the horizontal axis compared to the tethered condition (compare the right panels in Fig. 4B and C). A direct comparison of the tethered vs. untethered conditions showed that Oculus measures of grip aperture had significantly higher scaling ratio in the untethered compared to the tethered condition both for 3 cm and 5 cm objects (3 cm: statistic = 271, p-value = 0.003; 5 cm: statistic = 261, p-value = 0.005; Ansari-Bradley test). This was not the case for Optitrack measures of grip aperture for which, as expected, the scaling ratio of the distribution of the grip apertures was not significantly different between the tethered and untethered conditions for both the 3 cm and the 5 cm object (3 cm: statistic = 215, p-value = 1; 5 cm: statistic = 212, p-value = 0.94; Ansari-Bradley test).

The results of Fig. 4B, C suggest that, when the Oculus is tethered (Fig. 4B), the dispersion of its estimates of grip aperture is, at least for bigger objects (i.e. a 5 cm cylinder), not significantly different from that of Optitrack measurements. However, when the Oculus is untethered (Fig. 4C) the dispersion of its estimates of grip aperture are significantly larger than those provided by the Optitrack both for small and bigger objects. When the tethered and untethered conditions are directly compared the dispersion is significantly larger when the Quest moves together with the participant's head compared to when it rests on a tripod.

The Quest 2 provides noisy measures of acceleration

So far, we have focused on analyzing relevant events during reaching and grasping movements by considering their kinematic characteristics up to their first derivative (i.e. velocity). In this section, we broaden our analysis in two ways. First, we do not focus only on specific phases of the movement but we, more generally, consider its entire unfolding in time. Second, we do not stop at the first derivative but investigate the consistency between Oculus and Optitrack estimates of kinematic variables up to their second derivative (acceleration).

To address the two points above, we measured hand kinematics during the performance of two types of curvilinear hand movements: an ellipse (Fig. 5A) and a figure-of-eight (Figure S4A), and we assessed the reliability of Oculus-derived measures of acceleration by investigating whether they can be used to reveal the two-thirds power law, a kinematic invariant normally found in healthy human movements. In the following, we will discuss results obtained during performance of elliptical hand movements. Very similar results were obtained for figure-of-eight movements (Figure S4).

Figure 5B, C,D show the scatterplot of the instantaneous position, velocity, and acceleration of the wrist for one of the five repetitions. In all panels, the inset shows the slope of the linear fit and the R^2 value of this fit.

Estimates of hand position along the x and z axes provided by the Oculus were in virtually perfect agreement with their Optitrack ground-truth values throughout the movement both in the tethered and untethered conditions (Fig. 5B). Indeed, both the slope and R^2 of their linear fits were very close to 1 (Tethered - x: slope = 0.88, R^2 = 0.99; z: slope = 0.99, R^2 = 0.98 - Untethered: x: slope = 0.95, R^2 = 0.99; z: slope = 0.94, R^2 = 0.97 - average across all repetitions). However, in agreement with results in Fig. 2B, C, estimates of hand position along the y axis (the frontal direction in Fig. 2B, C) were noisier and, as a consequence, both the slope of the linear fit and the R^2 strongly deviated from 1 (Tethered - y: slope = 0.77, R^2 = 0.90 - Untethered: y: slope = 0.36, R^2 = 0.8 - average across all repetitions). These results indicate that the Oculus provides fairly accurate measures of position (i.e., $R^2 > 0.80$ and slope close to 1) in the left/right and up/down directions and it tends, however, to overestimate/underestimate the position along the close/far away direction during curvilinear hand movements. Indeed, in this direction, the Oculus underestimates the position of the hand when it is closer to the body, and it overestimates the position of the hand when it is far away from the body. The overall effect is a distortion of the veridical trajectory along the close/far away as shown in the bottom panel in Fig. 5A.

Oculus measures of velocity (Fig. 5C) followed the same pattern and they thus exhibited a closer match to their Optitrack ground-truth values along the x and z compared to the y axis both in the tethered and in the untethered conditions (Tethered - x: slope = 0.87, R^2 = 0.99; y: slope = 0.66, R^2 = 0.8; z: slope = 0.95, R^2 = 0.95 - Untethered: x: slope = 0.93, R^2 = 0.96; y: slope = 0.33, R^2 = 0.66; z: slope = 0.87, R^2 = 0.9 - average across all repetitions). Oculus estimates of velocity were thus still reliable ($R^2 > 0.8$ and slope close to 1), albeit noisy, along the left/right and up/down directions, although they tended to overestimate their Optitrack ground-truth values along the close/far away direction.

The accuracy of Oculus measures of acceleration (Fig. 5D) was also axis-dependent, with measures along the left/right axis being less noisy than along the up/down direction, which was, in turn, less noisy than along the close/far direction both in the tethered and untethered conditions (Fig. 5D). The average slope and R^2 of the linear fit between Oculus and Optitrack data, averaged across all 5 repetitions were: Tethered - x: slope = 0.78, R^2 = 0.87; y: slope = 0.3, R^2 = 0.37; z: slope = 0.63, R^2 = 0.62 - Untethered: x: slope = 0.71, R^2 = 0.72; y: slope = 0.17, R^2 = 0.26; z: slope = 0.44, R^2 = 0.45. To assess whether second derivatives estimated from Oculus position information could be used in kinematics assessments we computed the slope and the R^2 of the power-law that relates the radius of curvature (which depends on the second derivative) and instantaneous velocity (Fig. 5E). Log-log curvature-velocity plots derived from Oculus measures differred from those obtained from ground-truth Optitrack measures (compare left and right columns in Fig. 5E) and estimates of the slope and R^2 of their linear fits were slightly different in the two cases both in the tethered (Oculus: - slope=-0.21, R^2 = 0.57

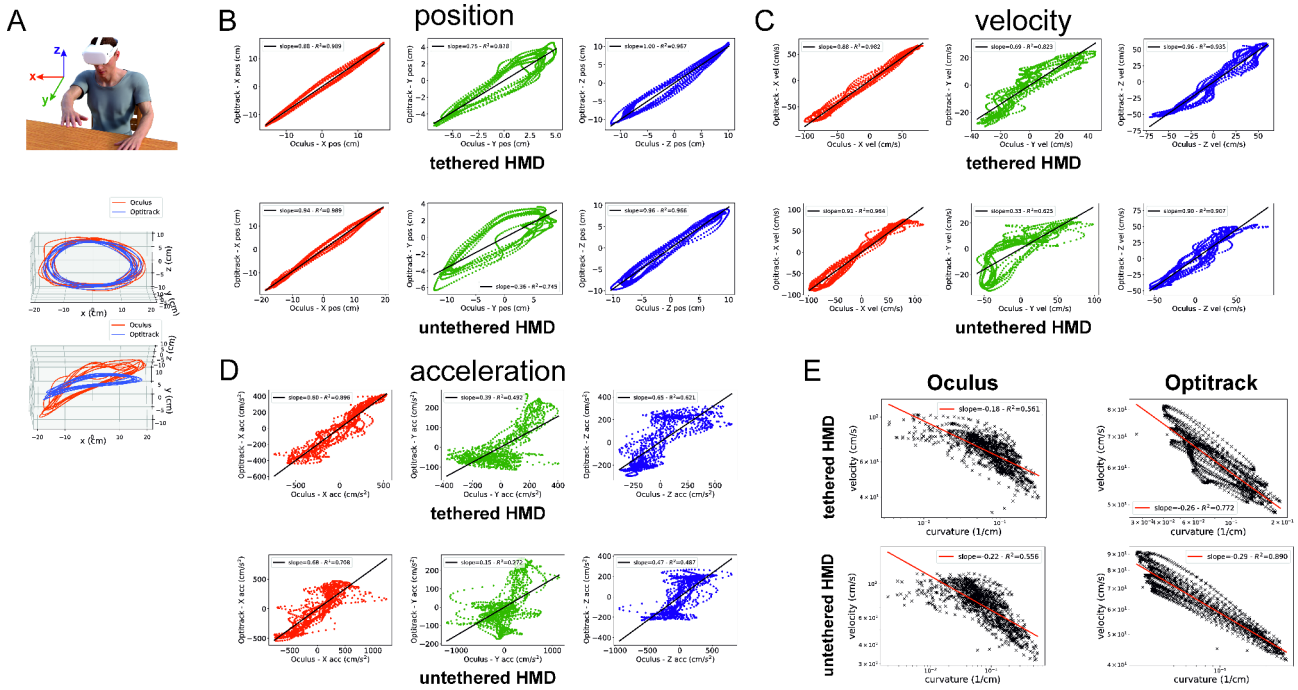

Fig. 5. Wrist position, velocity and acceleration during curvilinear hand movements – (**A**) Experimental paradigm. The subject executed elliptical hand movements in the air with his right hand. The curves in the bottom panel represent the position of the wrist during one of the experimental sessions. (**B**, **C**, **D**) Scatterplots of Oculus/Optitrack measures of wrist instantaneous position (B), velocity (C), and acceleration (C) along the x (left/right direction, red), y(close/far away direction, green) and z (top/down direction, blue) in the tethered (top row) and untethered (bottom row) conditions. Plotted data are from one out of five experimental sessions. In all panels, the black lines signify a linear fit of the data. The slope and R^2 of this fit are shown in the insert. (**E**) Scatterplot of the instantaneous curvature (x axis) against velocity (y axis) of the wrist measured from Oculus (left column) and Optitrack (right column) data in the tethered (top row) and untethered (bottom row) conditions. Results for the figure-of-eight trajectory are shown in Figure S4.

- Optitrack: slope=-0.26, $R^2 = 0.7$) and untethered (Oculus: - slope=-0.22, $R^2 = 0.59$ - Optitrack: slope=-0.27, $R^2 = 0.87$) conditions.

To further characterize how the Oculus estimates the hand kinematics characteristics during curvilinear movements we sampled the position, velocity and acceleration of the hand at points where the velocity was maximal (black dots in Fig. 6A) and minimal (black dots in Fig. 6B). These points were chosen because velocity (and acceleration) maxima and minima are often used to segment human movements[50,51] and, given the temporal periodicity of the performed movements, they were appropriately spaced in time not to be correlated by any of our necessary filtering procedures.

Results for points at velocity minima (Fig. 6A) in untethered condition are shown in Fig. 6B-D. The x component of the distances between pairs of consecutive points at local velocity maxima estimated from Oculus data was significantly higher compared to Optitrack data (Top panels in Fig. 6B. x: Oculus = 4.13 ± 2.9, Optitrack = 2.26 ± 1.7; y: Oculus = 2.1 ± 1.4, Optitrack = 2.1 ± 1.1; z: Oculus = 16.6 ± 2.8, Optitrack = 16.1 ± 1.8) and its scaling ratio significantly higher (x: statistic = 2380, p-value = 6.8 10^{-6}; y: statistic = 2789, p-value = 0.12; z: statistic = 2789, p-value = 0.12; Ansari-Bradley test). Optitrack and Oculus measures were correlated along the x and z, but not the y axis (bottom panels in Fig. 6B. x: $\rho = 0.49$, p-value = 6.2 10^{-6}, slope = 0.3, $R^2 = 0.51$; y: ρ=-0.03, p-value = 0.78, slope=-0.02, R^2=-0.02; z: $\rho = 0.87$, p-value = 3.5 10^{-25}, slope = 0.59, $R^2 = 0.91$ - p-values refer to Spearman's rank correlation).

In agreement with results in Figs. 2, 3, 4 and 5, Oculus-derived measurements of velocity (Fig. 6C) overestimated their Optitrack ground-truth values along all axes, with the overestimation along the y axis being the largest in percentage (x: Oculus = 81 ± 13, Optitrack = 79 ± 9.8; y: Oculus = 42 ± 16, Optitrack = 14 ± 3.7; z: Oculus = 15.2 ± 10, Optitrack = 7.3 ± 5.2). The scaling ratio across all axes was significantly larger for Oculus- compared to Optitrack-derived estimates (x: statistic = 3062, p-value = 0.02; y: statistic = 2581, p-vaue = 6.4 10^{-8}; z: statistic = 2791, p-value = 5.6 10^{-5}; Ansari-Bradley test). Optitrack and Oculus estimates of velocity were correlated along all three axes (bottom panels in Fig. 6B. x: $\rho = 0.74$, p-value = 1.4 10^{-15}, slope = 0.56, $R^2 = 0.75$; y: $\rho = 0.39$, p-value = 0.003, slope = 0.05, $R^2 = 0.24$; z: $\rho = 0.53$, p-value = 3.6 10^{-7}, slope = 0.21, $R^2 = 0.39$ – p-values refer to Spearman's rank correlation).

Similar to measurements of velocity, also Oculus-derived measurements of absolute acceleration overestimated their Optitrack ground-truth values along all axes (x: Oculus = 173 ± 189, Optitrack = 30.2 ± 21.3; y: Oculus = 164 ± 255, Optitrack = 109 ± 44; z: Oculus = 235 ± 193, Optitrack = 194 ± 60). The scaling ratio

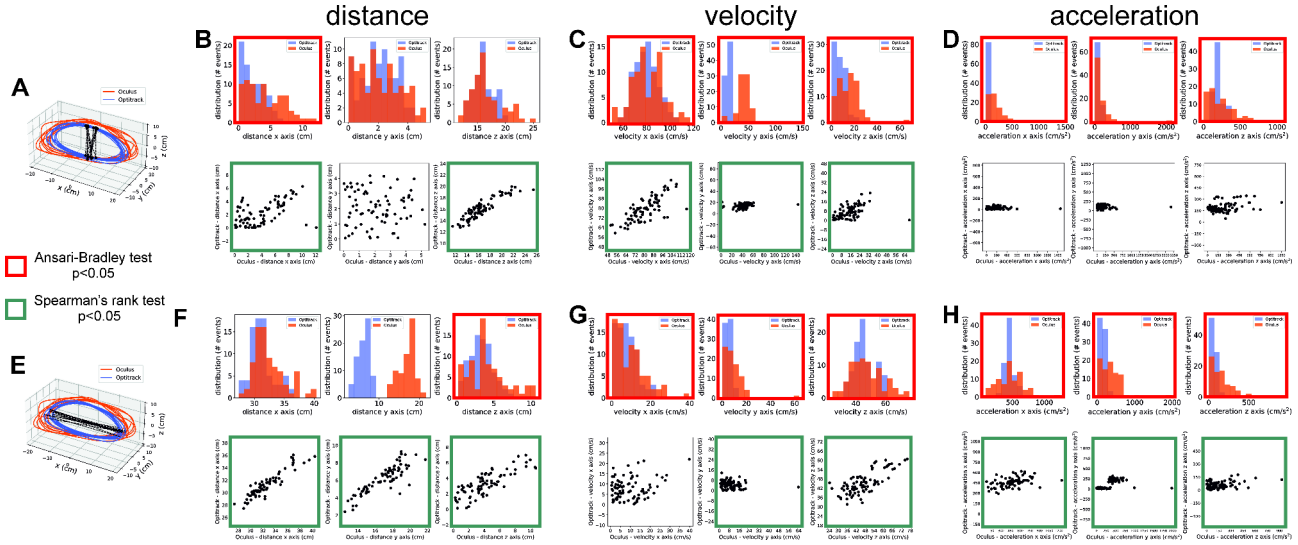

Fig. 6. Distance, velocity and acceleration measured at two different points along a curvilinear elliptical path – (**A**, **E**) Points of velocity maxima (black dots in panel A) and minima (black dots in panel E) where distance, velocity and acceleration were sampled. The dashed lines indicate the distance between consecutive pairs of points. (**B**) Distributions (top panels) and scatterplots (bottom panels) of the x, y and z components of distances measured between consecutive pairs of points of velocity maxima from Oculus and Optitrack data. (**C**, **D**) Distributions (top panels) and scatterplots (bottom panels) of the x, y and z components of the velocities and accelerations measured at points of velocity maxima from Oculus and Optitrack data. (**E**, **F**, **G**, **H**) Same as (A, B, C, D) for points at velocity minima.

across all axes was significantly larger for Oculus- compared to Optitrack-derived estimates (x: statistic = 2157, p-value = 2.5 10^{-16}; y: statistic = 2771, p-vaue = 3.2 10^{-5}; z: statistic = 2258, p-value = 5 10^{-14}; Ansari-Bradley test) and Optitrack and Oculus estimates of acceleration were not correlated along any of the axes (x: $\rho = 0.21$, p-value = 0.06, slope = 0.002, $R^2 = 0.02$; y: ρ=-0.2, p-value = 0.08, slope=-0.02, R^2=-0.13; z: $\rho = 0.21$, p-value = 0.06, slope = 0.1, $R^2 = 0.32$ – p-values refer to Spearman's rank correlation). The lack of correlation between Oculus and Optitrack measurements of acceleration is likely due to the fact that, in human hand movements, acceleration has a minimum at points of maximal velocity and, as also noted above, when the measured quantities are small Oculus' errors can be substantial.

Results for points at velocity minima (Fig. 6E) in untethered condition are shown in Fig. 6F-H. The y component of the distances between pairs of consecutive points at local velocity minima estimated from Oculus data was significantly higher compared to Optitrack data (Fig. 6F. x: Oculus = 32 ± 2.6, Optitrack = 31.1 ± 1.96; y: Oculus = 17 ± 2, Optitrack = 6.2 ± 1.5; z: Oculus = 4.2 ± 2, Optitrack = 3.3 ± 1.5). The scaling ratio across all axes was significantly larger for Oculus- compared to Optitrack-derived only for estimates along the z axis (x: statistic = 2883, p-value = 0.16; y: statistic = 2837, p-value = 0.08; z: statistic = 2747, p-value = 0.02; Ansari-Bradley test). Optitrack and Oculus measures of distance were correlated across all axes (bottom panels in Fig. 6F. x: $\rho = 0.89$, p-value = 5.5 10^{-28}, slope = 0.7, $R^2 = 0.92$; y: ρ=-0.81, p-value = 2.4 10^{-19}, slope=-0.63, R^2=-0.85; z: $\rho = 0.79$, p-value = 3.3 10^{-18}, slope = 0.49, $R^2 = 0.81$ - p-values refer to Spearman's rank correlation).

Oculus-derived measurements of velocity (Fig. 6G) overestimated their Optitrack veridical values across all axes, with the overestimation along the y axis being the largest in percentage (x: Oculus = 9.7 ± 7.8, Optitrack = 8 ± 5.1; y: Oculus = 9 ± 8.1, Optitrack = 4.7 ± 2.8; z: Oculus = 47 ± 11, Optitrack = 46 ± 7.2). The scaling ratio across all aces was significantly larger for Oculus- compared to Optitrack-derived estimates (x: statistic = 3105, p-value = 0.01; y: statistic = 2688, p-value = 2.6 10^{-7}; z: statistic = 3011, p-value = 0.002; Ansari-Bradley test) and Optitrack and Oculus estimates of velocity were correlated along the y and z but not the x axis (bottom panels in Fig. 6G. x: $\rho = 0.08$, p-value = 0.44, slope = 0.16, $R^2 = 0.25$; y: ρ=-0.22, p-value = 0.04, slope=-0.07, R^2=-0.19; z: $\rho = 0.69$, p-value = 8.4 10^{-13}, slope = 0.48, $R^2 = 0.74$ – p-values refer to Spearman's rank correlation).

Oculus-derived measurements of absolute acceleration overestimated their Optitrack veridical values along all axes (x: Oculus = 469 ± 200, Optitrack = 457 ± 69; y: Oculus = 350 ± 284, Optitrack = 121 ± 108; z: Oculus = 161 ± 153, Optitrack = 59 ± 39). The scaling ratio all axes was significantly larger for Oculus- compared to Optitrack-derived estimates (x: statistic = 2585, p-value = 6 10^{-9}; y: statistic = 2896, p-value = 0.0001; z: statistic = 2402, p-value = 2.6 10^{-12}; Ansari-Bradley test) and Optitrack and Oculus estimates of acceleration were correlated along all axes (x: $\rho = 0.51$, p-value = 1.1 10^{-6}, slope = 0.15, $R^2 = 0.44$; y: ρ=-0.69, p-value = 4 10^{-13}, slope = 0.19, $R^2 = 0.51$; z: $\rho = 0.23$, p-value = 0.03, slope = 0.09, $R^2 = 0.35$ – p-values refer to Spearman's rank correlation).

Results in Figs. 5 and 6 confirm, in agreement with Figs. 2, 3 and 4, that Oculus estimates of distances, velocity and acceleration are noisy and their variance is larger than that of their ground-truth values in almost all investigated conditions and along all axes (panels highlighted in red in Fig. 6). That said, Oculus estimates

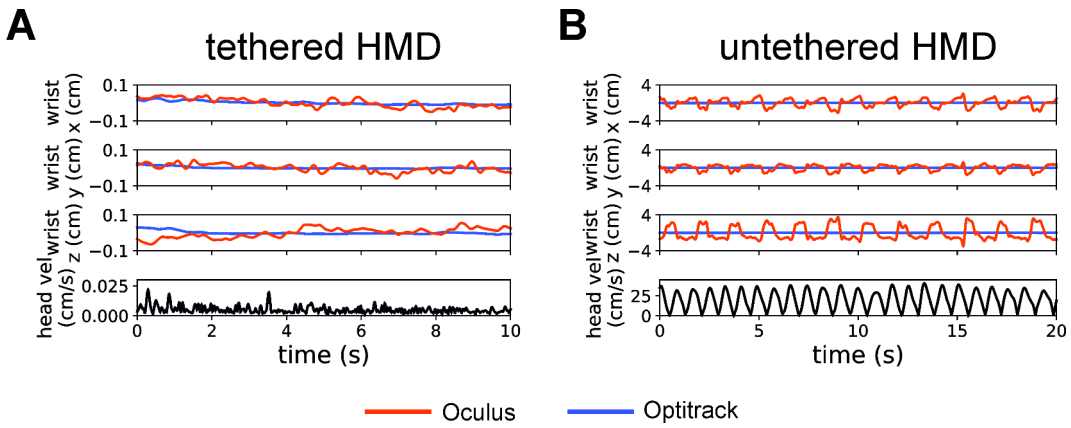

Fig. 7. Crosstalk between estimates of hand and head movements in the Oculus system – In both panels the top three plots show the x, y and z coordinates of a static hand recorded by the Oculus (red lines) and Optitrack (blue lines) systems, while the bottom plot show the HMD instantaneous velocity estimated from the Optitrack data. Panel A (condition *tethered HMD*) represents results obtained with a stationary HMD tethered to a tripod and panel B (condition *tethered HMD*) shows results obtained when the HMD was placed on the participant's head while he was bobbing it from side to side. Please notice the different scales used to plot results in the panel A and B respectively.

of both distance and velocity correlated (panels highlighted in green in Fig. 6), with very few exceptions, with their ground-truth values. Oculus estimates of acceleration, instead, correlated with their ground-truth values only at points of acceleration maxima (i.e. at velocity minima). Furthermore, the accuracy of Oculus estimates of distance appears to be axis-dependent (Fig. 5). Estimates along the left/right direction are the most accurate, followed by estimates along the top/down axis. Estimates along the near/far axis appear to be the noisiest. This measurement noise along the y axis was more pronounced in the untethered condition, where the R^2 of the linear fits of data was smaller than in the tethered condition.

Discussion

The goal of the present study was to quantitatively assess the accuracy and reliability of kinematic measures provided by the Oculus Quest 2 by comparing them to their ground-truth values measured by means of a marker-based high-quality commercial motion tracking system.

Overall, we found that the Quest 2 provides a reliable estimation of hand position and traveled distance both during center-out (Figs. 2 and 3) and curvilinear (Figs. 5 and 6) hand movements. The peak velocity estimates provided by the Oculus appeared to be less accurate than the position estimates, but they were still reliable, as they correlated with their ground-truth values in many, albeit not all, the investigated conditions (Fig. 6B, C,F, G). Finally, estimates of acceleration were the noisiest, exhibiting sometimes large deviations from their ground-truth values and, in many investigated conditions, they did not correlate with their ground-truth values (Fig. 6D). Notably, across all our experiments, we found that the precision of measured position (and thus velocity and acceleration) was axis-dependent, with estimates along the near/far axis being the noisiest. The algorithms that the Oculus uses to estimate hand position are patented and their details are not disclosed. Without such knowledge, any potential explanation would be highly speculative. That said, their quantitative investigation, as it is done here, may inform the design of motor rehabilitation tasks in virtual environments. For example, in cases when a good estimation of the participant's hand position is required, it would be preferable to have tasks that require movements along the frontal plane rather than tasks that require 'in-depth' movements.

Finally, the precision of grip aperture at the end of grasping movements, was a function of the size of the object and head movements (Fig. 4). Specifically, in the absence of head movements ("tethered" condition in Fig. 4), the precision of grip aperture estimates provided by the Oculus was not significantly different from ground-truth values for a larger (5 cm diameter) but not for a smaller (3 cm diameter) object. However, in the presence of head movements ("untethered" condition in Fig. 4), the precision of grip aperture estimates provided by the Oculus was larger than ground-truth values both for a larger and smaller object. A similar trend was found for measurements of travelled distances, that the Oculus measured more accurately in the tethered (Fig. 2B) compared to the untethered (Fig. 2C) condition. In both conditions, though, their dispersion was not significantly different from their ground-truth values. Notably, though, in all conditions Oculus estimates, albeit noisy, were significantly correlated with their ground-truth values.

In the present study, we considered only naturalistic ranges of head movements. As discussed above, such movements have the general effect of increasing the dispersion of Oculus measures that, in most of the investigated conditions, remained however significantly correlated with their ground-truth values. Our preliminary experiments show, however, that non-naturalistic head movements (e.g., bobbing the head from left to right continuously) can produce dramatic modulations of hand position (Fig. 7). In patients with abnormal patterns of head movements (e.g., diseases associated with tremor-like motor behavior), the estimates of hand movements might thus become very noisy and, importantly, potentially not correlated with their ground-truth

values. In these specific cases, one potential solution could be to have the patient act in the virtual environment by means of the two joysticks provided with the Oculus. These devices are provided with a set of independent accelerometers that allow the Oculus to, at least partially, disentangle hand from head movements. They could thus provide more reliable measurements of hand movements (see also[45,46]) at the expense, though, of a less naturalistic interaction in the virtual environment.

Limitations

One potential limitation of our study is that, in our experiments, we tested the precision of Quest 2's measures only in the presence of physiological head and hand movements (i.e. those of a healthy participant). Some pathologies that need motor rehabilitation (e.g., Parkinson's disease) might produce, in a subset of patients, excessive head/hand movements or tremor. Under these pathological conditions, a degradation of the precision of Quest 2's estimates is possible, rendering kinematic assessments less reliable/precise than in healthy participants. Future studies in patients are needed to fully explore this point (see, for example[47], for a first attempt).

A further potential limitation of our study is that, here, we analyzed a relatively small subset of data. Indeed, our data set consists of the position and rotation of all joints of the virtual hand fitted by the Quest 2 (see Table S1), and the trajectories of a set of 21 markers placed on all finger joints concurrently recorded by the Optitrack (Fig. 1). The main aim of the present study was to provide the reader with a clear and exhaustive description of how precisely and accurately the Oculus Quest estimates the hand position, velocity and acceleration. Our data set allows also to analyze more complex kinematic measures (e.g., kinematic synergies) that, for coherency purposes, were not reported here. Upon publication, we will make the full data set freely accessible to other groups. Thus, other groups could contribute to fully exploit the potential of our data set.

An additional potential limitation is represented by the limited number (i.e., two values) of cylinders' diameters used to investigate the accuracy of the Oculus in estimating the grip aperture (Fig. 4). Our experimental results provided evidence that the Oculus provides noisy estimation of grip aperture. However, our results with two object sizes do not allow us to conclusively assess how the error in estimating grip aperture depends on object size. In addition, the precision of the Oculus algorithms to recover hand posture might depend on the size of the subject's hand. Investigating that requires recording grasping movements performed by people with hands of different sizes. Further experiments are needed to fully explore these points.

Conclusion

Taken together, the results presented here suggest that Quest 2's estimates of hand position, velocity and grip aperture might be used for kinematic assessments. Indeed, although they exhibited biases (position), overestimation (velocity). and their precision was not homogeneous in space, they both correlated with their ground-truth values in almost all (position) or most (velocity) explored conditions. Therefore, in cases when a high accuracy in measuring patients' kinematics is not needed, it may be a potential alternative to more expensive motion tracking systems[47,52]. This might pave the way for the design of rehabilitation systems in which the Quest 2 is used as a cost-effective and portable device that not only displays rehabilitation scenarios in at-home settings while allowing the remote supervision of a therapist but it also provides on- or off-line kinematic assessments that can potentially inform medical decisions.

Methods

Subject

This study aimed to quantitatively assess the accuracy and precision of the Oculus Quest 2 in measuring human movements by using a commercial marker-based Optitrack system as the ground-truth benchmark. To this end, we need to collect a sufficiently high number of trials to be able to run statistical tests and repeat this process for different types of movements to investigate potential movement-specific inaccuracies of the Oculus system. Given this goal, collecting data for multiple subjects could be potentially detrimental as one would add to the intrinsic measurement variability of the Oculus also the extrinsic across-subject variability in performing movements. For this, reasons we chose to collect data from a single subject that, for practical reasons, was one of the authors (AC). The same choice was made in previous studies whose goal was, as is the case here, the technical benchmarking of a system[39,40,45,46]. All procedures were approved by the local Ethics Committees (Comitato Unico Provincia di Ferrara), were in accordance with the guidelines of the Declaration of Helsinki and were carried out with the participants' informed consent.

Experimental procedure

During the experiments, the participant sat in front of a table (Fig. 1A) and performed different hand actions, while a total of 21 reflective markers were applied on the main joints of the participant's right hand and 3 markers were applied on the head-mounted display. Figure 1B shows the positions and labels of all applied markers., In different experimental sessions the participant performed the following actions: center-out reaching movements, grasping actions on different objects and with different hand postures, and curvilinear hand movements.

In a preliminary assessment, the participant kept his hand still on the table, while bobbing his head, when wearing the Oculus Quest 2. This task was performed to investigate the crosstalk between estimates of the head and hand position.

During the center-out movements, the subject performed reaching movements from a central hand rest position to three different positions arranged to his left, frontally, and to his right (Fig. 3). 20 repetitions were performed for each reaching direction. On each trial, we computed, both from Oculus and Optitrack data, the movement length defined as the distance traveled by the hand from its starting to its final position.

During the grasping actions, the subject performed precision grips with his right index and thumb toward cylinders of two different diameters: 3 cm and 5 cm. For each object, 20 repetitions were performed. For each trial, we estimated the grip aperture from Oculus data by computing the distance between the position of the two joints *r_index_fingernail_marker_pos*, *r_thumb_fingernail_marker_pos* (Table S1) and from Optitrack data by computing the distance between the two markers *RIND3*, *RTMB2* (Fig. 1).

During the curvilinear hand movements, we measured hand kinematics during the performance of two types of curvilinear hand movements: an ellipse (Fig. 5A) and a figure-of-eight (Figure S4A). Each movement was performed five times, each time for 10s. We then computed estimates of hand instantaneous position, velocity, and acceleration from both Oculus and Optitrack data. To assess the reliability of Oculus-derived measures of acceleration we investigated whether they can be used to reveal the two-thirds power law normally found in healthy human movements.

All actions were performed in two experimental conditions, namely tethered and untethered. In the untethered condition, the participant wore the Oculus 2 (Meta, USA) head-mounted display (**HMD**) at the top of his head. This configuration allowed the participant to have a clear view of the table in front of him (Fig. 1A) and of the current position and movement of his hand to perform all movements in a naturalistic manner. In the tethered condition, the HMD was fixed on a tripod positioned in front of the participant's body. The participant's body posture was such that the Quest 2 was close to his head during action performance. This configuration still allowed the participant to perform all the required movements under naturalistic conditions, while maintaining, for the Oculus, the same field of view of the untethered condition.

Motion capture

During task execution, we recorded the participant's hand and head positions by means of the Oculus and of a commercial motion capture system (Optitrack, Natural Point Inc, Corballis, USA) equipped with 16 cameras. The Quest 2 estimates hand positions and postures by means of 4 on-board cameras. These cameras are placed at the corners of the HMD and they capture images of the participants' hands during task performance. The software running on the Oculus uses computer vision routines to segment the images of the hands from the background and to estimate their posture. The spatial location of the hands is computed by exploiting stereoscopic depth information provided by different cameras. The specific details of this process are patented, and they are thus not publicly available.

The Optitrack system uses a set of infrared cameras to track, by triangulation, the positions of a set of infrared-reflective markers. The precision of the system is set by means of a calibration procedure. The measurement error was < 0.1 mm throughout our sessions.

Similar to a previous study from our lab[47], to allow synchronization between the data recorded from the two systems, the Optirack system continuously broadcasted, in real-time, the unique identifier of each recorded frame of data on a local dedicated network. The Oculus Quest was connected to the same local dedicated network, it received this stream of data, and it used, in real time, each unique Optitrack frame identifier to timestamp the locally recorded kinematics data. This common temporal reference (i.e., Optitrack's frame identifiers) was off-line used to align the streams of data recorded by the Oculus and the Optitrack systems, prior to data analysis. Optitrack data were also off-line processed to interpolate gaps in the markers' position and then exported for further processing.

Data analysis

For both the Oculus and Optitrack data sets, velocity was obtained by differentiating position data and acceleration by differentiating velocity data. Acceleration is also used as an important kinematic marker. For example, it has been shown that, in the healthy population, the instantaneous radius of curvature, which is a function of acceleration, and velocity are related by a power-law relationship, the so-called two-thirds power law[53,54], during curvilinear hand motion[55–58]. Furthermore, in the clinical practice, jerk, an acceleration-derived quantity (see, for example[6]), , is used to assess motor functions.

All analyses were performed in Python version 3.12.2.

Most of the power of physiological human movements is usually confined to very low temporal frequencies (see, for example, Figure S3 in[57]). To remove measurement noise, we thus first low-pass filtered both Oculus and Optitrack data at 4 Hz by means of a 2nd order Butterworth filter, a step commonly performed in studies of human movements[57,59]. We then segmented both the Optitrack and Oculus data into trials by using the velocity profile of the wrist movements computed from Optitrack data during task performance. Specifically, a trial included all time frames in which the hand velocity was above a pre-defined threshold of 5 cm/s plus the time frames immediately preceding and following ranging, in different analyses, from 0 to 500 ms. Depending on the condition, we extracted and analyzed different kinematic features.

Static hand

In this condition, the participant held his hand stationary, and the wrist position and head velocity were analyzed in two different conditions: when the HMD was stationary on a tripod ("tethered" condition) and when the HMD was placed on the participant's head while he was bobbing it from side to side ("untethered" condition). This allowed to investigate the effect of the head movement, by stressing the motion acquisition system.

The wrist position was estimated from Optitrack data by averaging the positions of the RWRA and RWRB markers (Fig. 1B) and from Oculus data by extracting the position of the b_r_wrist_pos segment (see Table S1). The head velocity was estimated from Optitrack data by averaging the instantaneous velocities of the three markers HEADL, HEADR and HEADC (Fig. 1B).

In the tethered HMD condition, we analyzed a single 10s segment of data, while in the untethered HMD condition we analyzed five 20s segments of data.

Statistics

Kinematic measures obtained from Oculus data might be not normally distributed and/or contain outliers. For this reason, throughout this paper, we compared different conditions by means of non-parametric statistics. These statistics do not assume the normality of the underlying distributions and are robust to the presence of outliers.

Specifically, we used Wilcoxon signed rank test to compare the median of two distributions, Spearman's rank correlation to investigate correlation between samples from two distributions and Ansari-Bradley test[60], a non-parametric version of the F-test, to compare the scaling factor of two distributions, after removing the median from each one. When we fitted our data with a linear function, we also reported the associated coefficient of determination (R^2).

Preliminary test: crosstalk between measurements of hand and head movements in the Quest 2

The Oculus HMD tracks hand movements by filming the hands with its cameras, segmenting these images from the background and fitting these segmented images with a kinematic model (Table S1). Since the Oculus cameras move with the person's head, Meta has developed different hardware and software strategies to disentangle head from hand movements (i.e., accelerometers, heuristics, etc.). However smart and efficient these strategies are, they cannot necessarily be perfect. Thus, there are cases in which head movements are erroneously interpreted as hand movements.

To make this point clear, we conducted a preliminary test. In Fig. 7 we show the wrist position estimated by the Oculus and Optitrack systems when the Oculus was either tethered to a tripod (Fig. 7A, condition *tethered HMD*) or when it was worn by the participant while bobbing his head from side to side (Fig. 7B, condition *untethered HMD*).

Both Oculus (red curves in Fig. 7A) and Optitrack (blue curves in Fig. 7A) position estimates exhibited measurement errors along each axis that were bigger for the Oculus compared to the Optitrack (Oculus - standard deviation: x axis = 0.02 cm, y axis = 0.02 cm, z axis = 0.03 cm. Optitrack - standard deviation: x axis = 0.01 cm, y axis = 0.006 cm, z axis = 0.01 cm) and the ratio between the Oculus and Optitrack standard deviations was 2.5 along the x axis, 3.4 along the y axis and 2.8 along the z axis.

Figure 7B shows instead results obtained when the HMD was worn during periodic left-right bobbing movements of the head. In this condition, the estimates of the hand positions provided by the Oculus were dramatically more imprecise compared to the tethered conditions (Oculus - standard deviation: x axis = 0.87*cm*, y axis = 0.63 cm, z axis = 0.1.45 cm) and, most importantly, its variations correlated in time with the movements of the head (compare bottom black curve with red curves). As a consequence, the ratio between the Oculus and Optitrack standard deviations exhibited a dramatic increase and it was 38 along the x axis, 84 along the y axis and 246 along the z axis.

While the head-bobbing experimental condition is admittedly rather unusual and "extreme", it nonetheless clearly shows that, in the Oculus system, head movements can modulate estimates of hand movements.

Data availability

All code and data will be made available upon publication. The datasets generated and/or analyzed during the current study are also available from the corresponding author on reasonable request.

Received: 2 September 2024; Accepted: 21 February 2025
Published online: 14 March 2025

References

1. Slater, M. Place illusion and plausibility can lead to realistic behaviour in immersive virtual environments. *Philos. Trans. R. Soc. B Biol. Sci.* **364**, 3549–3557 (2009).
2. Slater, M. Immersion and the illusion of presence in virtual reality. *Br. J. Psychol.* **109**, 431–433 (2018).
3. Nenna, F., Do, C. T., Protzak, J. & Gramann, K. Alteration of brain dynamics during dual-task overground walking. *Eur. J. Neurosci.* **54**, 8158–8174 (2021).
4. Nenna, F., Zorzi, M. & Gamberini, L. Augmented reality as a research tool: Investigating cognitive-motor dual-task during outdoor navigation. *Int. J. Hum. Comput. Stud.* **152**, 102644 (2021).
5. Maymon, C., Grimshaw, G. & Wu, Y. C. *Virtual Reality in Behavioral Neuroscience: New Insights and Methods* (Springer International Publishing, 2023).
6. Maura, R. M. et al. BioMed Central,. Literature review of stroke assessment for upper-extremity physical function via EEG, EMG, kinematic, and kinetic measurements and their reliability. *J. NeuroEng. Rehabil.* **20** (2023).
7. Thrane, G., Sunnerhagen, K. S. & Murphy, M. A. Upper limb kinematics during the first year after stroke: The stroke arm longitudinal study at the university of Gothenburg (SALGOT). *J. Neuroeng. Rehabil.*. **17**, 76 (2020).
8. Kwakkel, G. et al. Standardized measurement of quality of upper limb movement after stroke: Consensus-based core recommendations from the second stroke recovery and rehabilitation roundtable. *Int. J. Stroke*. **14**, 783–791 (2019).
9. Lee, S. H., Jung, H., Yun, S. J., Oh, B. & Seo, H. G. Upper extremity rehabilitation using fully immersive virtual reality games with a head Mount display: A feasibility study. *PM R.* **12**, 257–262 (2020).
10. Yee, N. & Bailenson, J. The Proteus effect: The effect of transformed self-representation on behavior. *Hum. Commun. Res.* **33**, 271–290 (2007).
11. Marini, M. & Casile, A. I can see my virtual body in a mirror: The role of visual perspective in changing implicit Racial attitudes using VR. *Front. Psychol.* 1–10 https://doi.org/10.3389/fpsyg.2022.989582 (2022).
12. Bebko, A. O. & Troje, N. F. bmlTUX design and control of experiments in virtual reality and beyond. *Iperception* **11**, 1–12 (2020).
13. Tassinari, M., Aulbach, M. B. & Jasinskaja-Lahti, I. The use of virtual reality in studying prejudice and its reduction: A systematic review. *PLoS One*. **17**, e0270748 (2022).
14. Banakou, D., Groten, R. & Slater, M. Illusory ownership of a virtual child body causes overestimation of object sizes and implicit attitude changes. *Proc. Natl. Acad. Sci. USA* **110**, 12846–12851 (2013).

15. Burns, E. et al. The hand is slower than the eye: A quantitative exploration of visual dominance over proprioception. in *IEEE Virtual Reality Conference 2005 (VR'05)* vol. 3–10 (IEEE, 2005).
16. Anglin, J. M., Sugiyama, T. & Liew, S. L. Visuomotor adaptation in head-mounted virtual reality versus conventional training. *Sci. Rep.* **7**, 1–8 (2017).
17. Van Loon, A., Bailenson, J., Zaki, J., Bostick, J. & Willer, R. Virtual reality perspective-taking increases cognitive empathy for specific others. *PLoS One*. **13**, 1–19 (2018).
18. Bozzacchi, C. & Domini, F. Lack of depth constancy for grasping movements in both virtual and real environments. *J. Neurophysiol.* **114**, 2242–2248 (2015).
19. Maselli, A., De Pasquale, P., Lacquaniti, F. & D'Avella, A. Interception of virtual throws reveals predictive skills based on the visual processing of throwing kinematics. *iScience* **25**, 105212 (2022).
20. Borzelli, D., Cesqui, B., Berger, D. J., Burdet, E. & D'Avella, A. Muscle patterns underlying voluntary modulation of co-contraction. *PLoS One*. **13**, 1–30 (2018).
21. Gurgone, S. et al. Simultaneous control of natural and extra Degrees-of-Freedom by isometric force and EMG null space activation. *Biosyst Biorobotics*. **28**, 863–868 (2022).
22. Fodor, L. A. et al. The effectiveness of virtual reality based interventions for symptoms of anxiety and depression: A meta-Analysis. *Sci. Rep.* **8**, 1–13 (2018).
23. Keizer, A., Van Elburg, A., Helms, R. & Dijkerman, H. C. A virtual reality full body illusion improves body image disturbance in anorexia nervosa. *PLoS One*. **11**, 1–21 (2016).
24. Rose, F. D., Brooks, B. M. & Rizzo, A. A. Virtual reality in brain damage rehabilitation: Review. *Cyberpsychology Behav.* **8**, 241–262 (2005).
25. Maggio, M. G. et al. Do patients with neurological disorders benefit from immersive virtual reality? A scoping review on the emerging use of the computer-assisted rehabilitation environment. *Eur. J. Phys. Rehabil. Med.* **60**, 37–43 (2024).
26. Pau, M. et al. Effect of immersive virtual reality training on hand-to-mouth task performance in people with multiple sclerosis: A quantitative kinematic study. *Mult Scler. Relat. Disord*. **69**, 104455 (2023).
27. Demeco, A. et al. Immersive virtual reality in post-stroke rehabilitation: A systematic review. *Sensors* **23**, 1712 (2023).
28. Foley, N. et al. Are recommendations regarding inpatient therapy intensity following acute stroke really evidence-based? *Top. Stroke Rehabil.*. **19**, 96–103 (2012).
29. Sampaio-Baptista, C., Sanders, Z. B. & Johansen-Berg, H. Structural plasticity in adulthood with motor learning and stroke rehabilitation. *Annu. Rev. Neurosci.* **41**, 25–40 (2018).
30. Veerbeek, J. M. et al. What is the evidence for physical therapy poststroke? A systematic review and meta-analysis. *PLoS One* **9**, e87987 (2014).
31. Paolucci, S. et al. Impact of participation on rehabilitation results: A multivariate study. *Eur. J. Phys. Rehabil Med.* **48**, 455–466 (2012).
32. Zampolini, M. et al. Tele-rehabilitation: present and future. *Ann. Ist Super Sanita*. **44**, 125–134 (2008).
33. Fregna, G., Schincaglia, N., Baroni, A., Straudi, S. & Casile, A. A novel immersive virtual reality environment for the motor rehabilitation of stroke patients: A feasibility study. *Front. Robot AI*. **9**, 1–12 (2022).
34. Crosbie, J. H., Lennon, S., McGoldrick, M., McNeill, M. & McDonough, S. Virtual reality in the rehabilitation of the arm after hemiplegic stroke: A randomized controlled pilot study. *Clin. Rehabil.* **26**, 798–806 (2012).
35. Ögün, M. N. et al. Effect of leap Motion-based 3D immersive virtual reality usage on upper extremity function in ischemic stroke patients. *Arq. Neuropsiquiatr.* **77**, 681–688 (2019).
36. Mekbib, D. B. et al. A novel fully immersive virtual reality environment for upper extremity rehabilitation in patients with stroke. *Ann. N Y Acad. Sci.* **1493**, 75–89 (2021).
37. Fregna, G. et al. Head-Mounted displays for upper limb stroke rehabilitation: A scoping review. *J. Clin. Med.* **12**, 7444 (2023).
38. De Pasquale, P., Bonanno, M., Mojdehdehbaher, S., Quartarone, A. & Calabrò, R. S. The Use of head-mounted display systems for upper limb kinematic analysis in post-stroke patients: A perspective review on benefits, challenges and other solutions. *Bioengineering* **11**, (2024).
39. Carnevale, A. et al. Virtual reality for shoulder rehabilitation: accuracy evaluation of oculus Quest 2. *Sensors* **22**, 5511 (2022).
40. Nie, J. Z., Nie, J. W., Hung, N. T., Cotton, R. J. & Slutzky, M. W. Portable, open-source solutions for estimating wrist position during reaching in people with stroke. *Sci. Rep.* **11**, 22491 (2021).
41. Kourtesis, P., Collina, S., Doumas, L. A. A. & MacPherson, S. E. Technological competence is a Pre-condition for effective implementation of virtual reality head mounted displays in human neuroscience: A technological review and meta-analysis. *Front. Hum. Neurosci.* **13**, 1–17 (2019).
42. Kelly, J. W., Doty, T. A., Ambourn, M. & Cherep, L. A. Distance perception in the oculus Quest and oculus Quest 2. *Front. Virtual Real.* **3**, 1–7 (2022).
43. Holzwarth, V., Gisler, J., Hirt, C. & Kunz, A. Comparing the accuracy and precision of SteamVR tracking 2.0 and oculus Quest 2 in a room scale setup. in *The 5th International Conference on Virtual and Augmented Reality Simulations* 42–46 (ACM, 2021). https://doi.org/10.1145/3463914.3463921
44. Boulo, J., Blanchette, A. K., Cyr, A. & McFadyen, B. J. Validity and reliability of the tracking measures extracted from the oculus Quest 2 during locomotion. *Comput. Methods Biomech. Biomed. Eng. Imaging Vis.* **12**, 257 (2024).
45. Pereira, D., Oliveira, V., Vilaça, J. L., Carvalho, V. & Duque, D. Measuring the precision of the oculus Quest 2's handheld controllers. *Actuators* 12, (2023).
46. Rojo, A. et al. Accuracy study of the oculus touch v2 versus inertial sensor for a single-axis rotation simulating the elbow's range of motion. *Virtual Real.* **26**, 1651–1662 (2022).
47. Casile, A. et al. Quantitative comparison of hand kinematics measured with a markerless commercial head-mounted display and a marker-based motion capture system in stroke survivors. *Sensors* **23**, (2023).
48. Krakauer, J. W., Hadjiosif, A. M., Xu, J., Wong, A. L. & Haith, A. M. Motor learning. in *Comprehensive Physiology* vol. 9, pp. 613–663 (Wiley, 2019).
49. Schwarz, A., Kanzler, C. M., Lambercy, O., Luft, A. R. & Veerbeek, J. M. Systematic review on kinematic assessments of upper limb movements after stroke. *Stroke* **50**, 718–727 (2019).
50. Fod, A., Matarić, M. J. & Jenkins, O. C. Automated derivation of primitives for movement classification. *Auton. Robots*. **12**, 39–54 (2002).
51. Hemeren, P. E. & Thill, S. Deriving motor primitives through action segmentation. *Front. Psychol.* **1**, 1–11 (2011).
52. Longo, U. G. et al. Immersive virtual reality for shoulder rehabilitation: evaluation of a physical therapy program executed with oculus Quest 2. *BMC Musculoskelet. Disord.*. **24**, 1–11 (2023).
53. Viviani, P. & Terzuolo, C. Trajectory determines movement dynamics. *Neuroscience* **7**, 431–437 (1982).
54. Lacquaniti, F., Terzuolo, C. & Viviani, P. The law relating the kinematic and figural aspects of drawing movements. *Acta Psychol. (Amst)*. **54**, 115–130 (1983).
55. Levit-Binnun, N., Schechtman, E. & Flash, T. On the similarities between the perception and production of elliptical trajectories. *Exp. Brain Res.* **172**, 533–555 (2006).
56. Dayan, E. et al. Neural representations of kinematic laws of motion: evidence for action-perception coupling. *Proc. Natl. Acad. Sci. U S A*. **104**, 20582–20587 (2007).
57. Casile, A. et al. Neuronal encoding of human kinematic invariants during action observation. *Cereb. Cortex*. **20**, 1647–1655 (2010).

58. Agosta, S., Battelli, L. & Casile, A. Human movements and abstract motion displays activate different processes in the observer's motor system. *Neuroimage* **130**, 184–193 (2016).
59. Schaal, S. & Sternad, D. Origins and violations of the 2/3 power law in rhythmic three-dimensional arm movements. *Exp. Brain Res.* **136**, 60–72 (2001).
60. Ansari, A. R. & Bradley, R. A. Rank run tests for disperson. *Ann. Math. Stat.* **31**, 1174–1189 (1960).

Acknowledgements

This work was partially supported by the Italian Ministry of Health, Piano Operativo Salute (POS) Trajectory 2 through the project "Rete eHealth: AI e strumenti ICT Innovativi orientati alla Diagnostica Digitale (rAIdD)" (code T2-AN-04 - CUP J43C22000380001).

Author contributions

A.C. and D.B. conceived the experiment, A.C. and V.B. conducted the experiment. A.C., V.B. and D.B. analyzed the results.A.C. and D.B. drafted the manuscript. All authors reviewed and approved the final manuscript.

Declarations

Competing interests

The authors declare no competing interests.

Additional information

Supplementary Information The online version contains supplementary material available at https://doi.org/10.1038/s41598-025-91552-5.

Correspondence and requests for materials should be addressed to A.C.

Reprints and permissions information is available at www.nature.com/reprints.

Publisher's note Springer Nature remains neutral with regard to jurisdictional claims in published maps and institutional affiliations.

Open Access This article is licensed under a Creative Commons Attribution-NonCommercial-NoDerivatives 4.0 International License, which permits any non-commercial use, sharing, distribution and reproduction in any medium or format, as long as you give appropriate credit to the original author(s) and the source, provide a link to the Creative Commons licence, and indicate if you modified the licensed material. You do not have permission under this licence to share adapted material derived from this article or parts of it. The images or other third party material in this article are included in the article's Creative Commons licence, unless indicated otherwise in a credit line to the material. If material is not included in the article's Creative Commons licence and your intended use is not permitted by statutory regulation or exceeds the permitted use, you will need to obtain permission directly from the copyright holder. To view a copy of this licence, visit http://creativecommons.org/licenses/by-nc-nd/4.0/.

© The Author(s) 2025